Hindawi
Mathematical Problems in Engineering
Volume 2021, Article ID 5520029, 12 pages
https://doi.org/10.1155/2021/5520029

Research Article

Analysis and Optimization of Static Contact Characteristics of Heavy-Duty Tracked Vehicle Rollers

He Tian,[1] **Yi Fang**,[1] **Shuai Wang**,[2] **Zeren Chen**,[1] **and Chuliang Yan**[1]

[1]*School of Mechanical and Aerospace Engineering, Jilin University, Changchun, China*
[2]*State Key Laboratory of Internet of Things for Smart City and Department of Electrical and Computer Engineering, University of Macau, Macao, China*

Correspondence should be addressed to Yi Fang; fangyi7012@163.com

Received 11 January 2021; Revised 26 March 2021; Accepted 9 April 2021; Published 26 April 2021

Academic Editor: Gabriel Luque

The static contact characteristics of heavy-duty tracked vehicle roller and track plate contact structure are analyzed, and the influence mechanism of the roller's shape parameters on the contact stress is studied. According to the Hertz contact theory, a mathematical model of the roller and track plate contact is established. The contact structure model is established in ANSYS software, and the simulation results are compared with the Hertz theory results to verify each other. In the parameter optimization section for the roller and track plate, based on the Hertz stress calculation formula, a new method is proposed to establish a roller and track plate Kriging model and to globally optimize the model by the genetic algorithm (GA). After that, the relationship among the track roller radius R_1, the track roller rim radius r_1, and the track plate rim radius r_2 is analyzed. The results show that the difference between the radius of the rim of the roller and the track plate and the radius of the roller rim both affect the maximum contact stress. Changing the plane contact into the curved surface contact can reduce the maximum contact stress by 33%. This study can provide a reference for the design and manufacture of supporting track rollers and track plates.

1. Introduction

The crawler tracking mechanism is widely used in heavy construction vehicles. Compared with the wheeled walking device, it can effectively ensure the stability of the whole machine and has the advantages of large traction and low specific pressure to the ground. The track roller is an important component of the crawler walking device, which supports the weight of the whole machine. However, its working environment is harsh, and the load is complex. If it fails, it will affect the overall work safety and work efficiency of the vehicle. Therefore, it is important to research the contact characteristics such as the roller load distribution pattern and relevant influencing factors.

In recent years, many scholars have studied the contact problems of the track roller. Arsic et al. [1] analyzed the failure causes of the ARs 2000 track roller of the superlarge reclaimer and found that the root cause lies in the defects of design and manufacture by means of theoretical calculation, numerical simulation, and experiments. Zhao J [2] analyzed the line contact stress of the drive wheel by the finite-element method to obtain the maximum load capacity. The Kriging model has been widely used to calculating complex models in recent years [3–5]. Zhang G [6] used the Kriging model combined with a genetic algorithm to optimize the reliability of gear transmission in large ball mills.

In the project, the Hertz contact theory is often used to calculate the roller's contact stress. The Hertz contact theory is also widely used in other similar structures, such as the wheel-rail contact of the train [7–10], the contact between the rolling element in the bearing and the inner and outer rings of the bearing [11,12], the calculation of the gear meshing stress [13–18], and the contact relationship between the inner and outer rings of angular contact ball bearings [19,20].

Although many researchers have studied the calculation method of the relationship between the track roller and the load, they have neglected the influence of the structural

parameters of the crawler support wheel and the curved surface size of the crawler plate on the maximum contact stress. Therefore, based on studying the contact stress and equivalent stress in the contact area, this paper analyses the relationship between the structural parameters of the crawler support wheel and the crawler plate, establishes the Kriging model, and uses the genetic algorithm to optimize it, to reduce the contact stress between the heavy track roller and the track plate.

In the first part of this paper, the contact mathematical model between the roller and track plate is established by using the Hertz contact theory of arbitrary curved surface contact. Figure 1(a) is the point contact model picture of the roller and the track plate, and Figure 1(b) is the enlarged cross-sectional view of the point contact area. The second part uses 3D software to model the roller and track plate and simulates it in finite-element software ANSYS. The obtained simulation data are compared with the calculation data of the Hertz formula, and the correctness of the Hertz formula is verified. In the third and fourth parts, the Kriging model is established, and genetic algorithm is used to optimize the model. The fifth part is the characteristic analysis between the structural parameters of the roller and the track plate. The final part is the summary of the full text.

2. Hertz Contact Theory

Based on the Hertz contact theory of arbitrary surface contact in modern contact mechanics, the surface near the contact point can be approximated as a paraboloid [21]. According to the elastic contact theory formula, the contact stress calculation method of the contact surface of the roller and the curved surface of the track plate can be introduced as follows [22].

When any surface I and surface II are in elastic contact, since the surface near the contact point can be approximated as a paraboloid, any coordinate with O as the origin can be expressed as follows:

$$\begin{aligned} \text{I: } z_1 &= A_1x^2 + A_2xy + A_3y^2, \\ \text{II: } z_2 &= B_1x^2 + B_2xy + B_3y^2. \end{aligned} \tag{1}$$

The coordinate system is established as shown in Figure 1(c).

The roller equation can be expressed as

$$z_1(x, y) = -\sqrt{\left(\sqrt{r_1^2 - x^2} + R - r_1\right)^2 - y^2} + R_1. \tag{2}$$

The track plate equation can be expressed as

$$z_2(x, y) = \sqrt{r_2^2 - x^2} - r_2. \tag{3}$$

In the model, r_1 is the radius of the roller rim, r_2 is the radius of the cylindrical surface of the track plate, and R_1 is the radius of the track roller.

Considering that the contact between the roller and the track plate is only in a small area near the origin, the equation can be expanded according to the second-order Taylor formula at $x = y = 0$:

$$z_1(x, y) = z_1(0, 0) + x\frac{\partial z_1}{\partial x} + y\frac{\partial z_1}{\partial y} + \frac{1}{2}\left[x^2\frac{\partial^2 z_1}{\partial x^2}\bigg|_0 + xy\frac{\partial^2 z_1}{\partial x\,\partial y}\bigg|_0 + y^2\frac{\partial^2 z_1}{\partial y^2}\bigg|_0\right] + \cdots, \tag{4}$$

$$z_2(x, y) = z_2(0, 0) + x\frac{\partial z_2}{\partial x} + y\frac{\partial z_2}{\partial y} + \frac{1}{2}\left[x^2\frac{\partial^2 z_2}{\partial x^2}\bigg|_0 + xy\frac{\partial^2 z_2}{\partial x\,\partial y}\bigg|_0 + y^2\frac{\partial^2 z_2}{\partial y^2}\bigg|_0\right] + \cdots. \tag{5}$$

Since the plane XOY passes through the tangent point and is a cotangent plane of two surfaces, the first partial derivative is 0; then,

$$\begin{aligned} &\frac{\partial^2 z_1}{\partial x^2}\bigg|_0 = \frac{1}{r_1}, \frac{\partial^2 z_1}{\partial y^2}\bigg|_0 = \frac{1}{R_1}, \frac{\partial^2 z_2}{\partial x^2}\bigg|_0 = -\frac{1}{r_2}, \frac{\partial^2 z_2}{\partial y^2}\bigg|_0 = 0, \\ &\frac{\partial^2 z_1}{\partial x\,\partial y}\bigg|_0 = \left(\sqrt{r_1^2 - x^2} + R - r_1\right)\left(r_1^2 - x^2\right)^{-1/2} x\left[\left(\sqrt{r_1^2 - x^2} + R - r_1\right)^2 - y^2\right]^{-3/2} y\bigg|_0 = 0. \end{aligned} \tag{6}$$

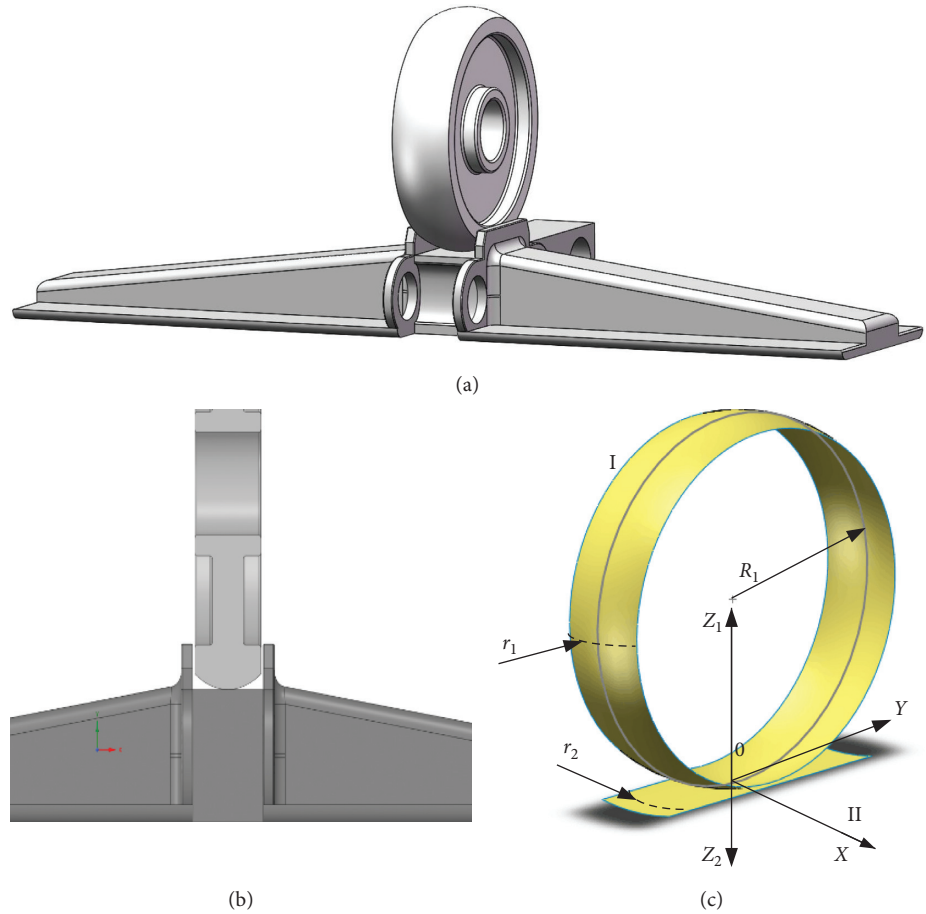

Figure 1: Point contact between the roller and track plate model.

Similarly, $\partial^2 z_2/\partial x\,\partial y| = 0$.

Then, the abovementioned two equations can be rewritten as

$$z_1 = \frac{1}{2}\left(\frac{1}{r_1}x^2 + \frac{1}{R_1}y^2\right), \tag{7}$$

$$z_2 = \frac{1}{2}\left(-\frac{1}{r_2}x^2\right). \tag{8}$$

Adding equations (7) and (8), we get

$$z_1 + z_2 = \frac{1}{2}\left[\left(\frac{1}{r_1} - \frac{1}{r_2}\right)x^2 + \frac{1}{R_1}y^2\right]. \tag{9}$$

We make $A = (1/r_1 - 1/r_2), B = 1/R_1$.

Formula (9) can be written as

$$z_1 + z_2 = Ax^2 + By^2. \tag{10}$$

In Hertz theory, it is assumed that the contact area between arbitrary continuous surfaces is elliptical. Using the point displacement formula of the elastic half-space surface [23],

$$(w)_0 = \frac{3P}{2\pi a}\frac{1-v^2}{E}\left[K(k) - D(k)\frac{x^2}{a^2} - C(k)\frac{y^2}{b^2}\right]. \tag{11}$$

Among them, K(k) and E(k) are the first class and the second class is elliptic integral. Elliptical eccentricity $k = \sqrt{1-(b/a)^2}$; elliptical integrated score: $D(k) = 1/k^2[K(k) - E(k)]$, $C(k) = 1/k^2[E(k) - (1-k^2)K(k)]$.

From the geometric relationship of the contact area deformation,

$$h(x, y) = (z_1 + \delta_1) + (z_2 + \delta_2). \tag{12}$$

Bringing (10) and (11) into equation (12),

$$\delta = Ax^2 + By^2 + \frac{3P}{2\pi a}\frac{1-v^2}{E}\left[K(k) - D(k)\frac{x^2}{a^2} - C(k)\frac{y^2}{b^2}\right] \cdot \left(\frac{1-v_1^2}{E_1} + \frac{1-v_2^2}{E_2}\right). \tag{13}$$

According to the method of undetermined coefficients,

$$\delta = \left(\frac{1-v_1^2}{E_1} + \frac{1-v_2^2}{E_2}\right) K(k) \frac{3P}{2\pi a}, \tag{14}$$

$$A = \left(\frac{1-v_1^2}{E_1} + \frac{1-v_2^2}{E_2}\right) \frac{D(k)}{a^2} \frac{3P}{2\pi a}, \tag{15}$$

$$B = \left(\frac{1-v_1^2}{E_1} + \frac{1-v_2^2}{E_2}\right) \frac{C(k)}{b^2} \frac{3P}{2\pi a}. \tag{16}$$

We define $\eta = (1 - v_1^2/E_1 + 1 - v_2^2/E_2)$.
From (14)–(16), we can get

$$a = \sqrt[3]{\frac{3}{2}\eta \frac{P}{\pi A} D}, \tag{17}$$

$$b = \sqrt{\frac{A}{B} \frac{(K-D)}{D}} \sqrt[3]{\frac{3}{2}\eta \frac{P}{\pi A} D}, \tag{18}$$

$$q_{\max} = \frac{3}{2} \frac{P}{\pi a b}. \tag{19}$$

3. Simulation and Verification

We are going to explore the maximum stress on the contact point of the roller and find the influence of geometric parameters on stress. To simplify the calculation, only the area near the contact point is modeled for static analysis, and the ANSYS software is used to build the structural 3D solid model. The dimensional parameters related to the roller and the track plate are shown in Table 1.

Figure 2 shows the finite-element model of the roller and track plate in ANSYS. The material of the simulation model is G42CrMo4, the density is 7850 kg/m3, Poisson's ratio is 0.3, and the elastic modulus is 2.1e1011. Before the finite-element calculation, the contact model needs to be meshed. The point contact area between the roller and the track plate is the key area in the analysis and calculation. The meshing of the contact area directly affects the accuracy, speed, and correctness of the calculation results. As shown in Figure 2(a), analysis model for the simulation of meshing diagram, the figure of the roller and crawler board of grid unit types for Solid186 and Solid186 is an advanced 3d 20-node fixed structure unit; each node has three translational degrees of freedom, along the direction of the unit with arbitrary spatial anisotropy, and supports the plasticity, superelasticity, creep, stress players, large deformation, and large strain capacity [24]. In the finite-element simulation, the contact area of the model was divided into meshes three times after the initial mesh refinement. After the mesh refinement, the simulation model had 205000 nodes and 146776 elements, and the element size of the contact area was 3.75 mm. Figure 2(b) shows the schematic diagram of the loading load and constraints of the simulation model. The red arrow indicates that constraints are established on this surface. For surfaces 1#, 2#, and 3#, the degree of freedom in the Y-direction is constrained; for surface 4#, the degree of freedom in all directions includes the degree of freedom in the X-, Y-, and Z-direction and the rotational degree of freedom around three axes. The pink arrow represents the Dutch way of loading; to simulate the actual working condition of roller center aperture by a load of shaft sleeve, the way of the linear strain of the beam element is used in the simulation of the applied load, the beam element Beam188 is a two-node unit, very suitable for linear, large-angle rotation, and is not a linear large strain, and establishing with beam element load can be evenly distributed to the inner surface of roller diameter of 567 nodes [24].

Table 1: Size of the track roller and track plate.

Parameter	Notation	Value
Track roller radius	R1	0.6 m
Track roller rim radius	r1	0.5 m
Track roller width	B1	0.2 m
Track plate radius	R2	∞
Track plate rim radius	r2	0.8 m
Track plate width	B2	0.2 m
Elastic modulus	E	206 GPa

Under the condition of the abovementioned model setting, the roller's maximum stress is studied by loading the pressure from 400 kN to 2000 kN. When the normal load is 1200 kN, the pressure distribution in the contact area is shown in Figure 3. The contact area is oval, and the maximum contact pressure is at the center of the ellipse, which is consistent with Hertzian contact theory. The equivalent stress distribution is shown in Figure 4.

To ensure the bearing capacity of the track plate structure is sufficient, the contact stress and equivalent stress value of the load are calculated to ensure that the strength meets the strength theory requirements. Table 2 shows the theoretical values of Hertzian contact, finite-element simulation contact stress value, and equivalent stress value for five different magnitudes of pressure from 400 kN to 2000 kN. According to the analysis of Table 2 and Figure 5, it shows that the maximum contact stress values are similar. The result proves the rationality of the model and the correctness of the simulation results.

According to the design manual [25], the roller and track plate are made of cast steel quality grade materials. The material used is G42CrMo4, with a yield strength of 900 MPa. The contact stress is divided into static and dynamic stress, and static and dynamic allowable contact stresses are $p_{\text{Hper,sta}}$ = 2000MPa and $p_{\text{Hper,dyn}}$ = 1078MPa. Only static contact stress is considered in this paper. As shown in Table 2, when the load is 400 KN, 800 KN, 1200 KN, 1600 KN, and 2000 KN, the contact stress values calculated by the Hertz formula and ANSYS are lower than the allowable static contact stress value of 2000 MPa. According to Table 3, when the load is 1200 KN, 1600 KN, and 2000 KN, although the contact stress meets the strength requirement, the internal equivalent stress of the roller and the track plate has exceeded the yield strength value of 900 MPa and exceeds 3.56%, 15.56%, and 23.33%, respectively. In this case, the roller and the track plate will be plastically deformed, which is prone to breakage and damage. Therefore, the structural parameters of the roller

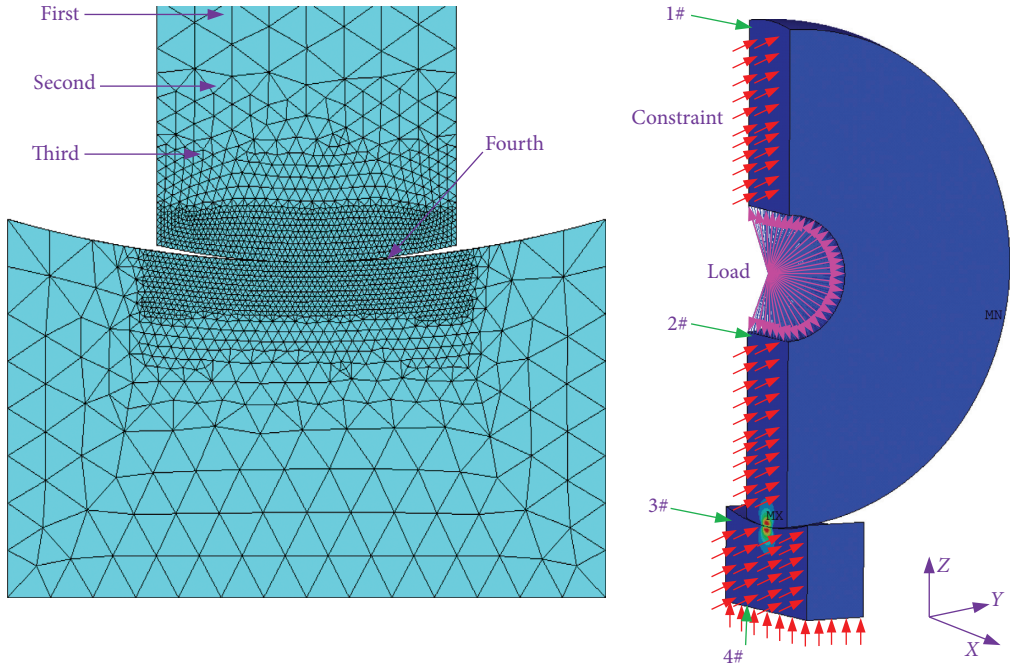

Figure 2: Finite-element model.

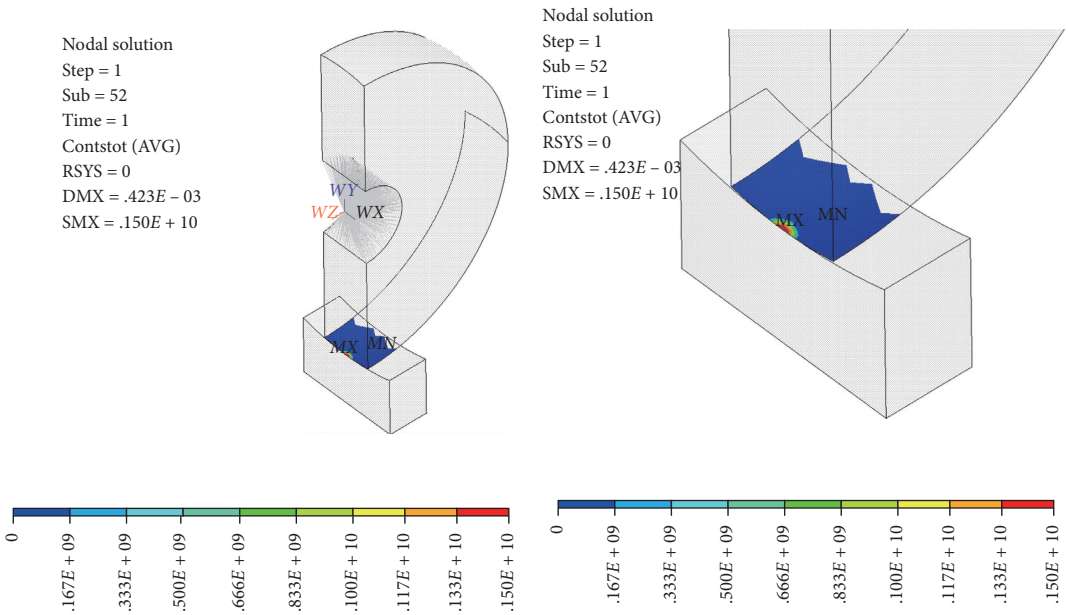

Figure 3: Contact pressure distribution.

and track plates should be optimized to meet the strength requirements.

4. Optimization and Analysis

Hertz stress calculation formula is relatively complex, including the first kind, the second kind of elliptic integral, and the transcendental equation, and its parameter values are conditionally limited and the calculation time will be relatively long, which cannot guarantee the correctness of the calculation result. Therefore, based on the Hertz stress calculation formula, a roller and track plate Kriging model is established, and the model is optimized by genetic algorithm.

4.1. Establishment of the Kriging Model. The Kriging method [26,27] is mainly used for the estimation problem in two-dimensional and three-dimensional space, that is, using a

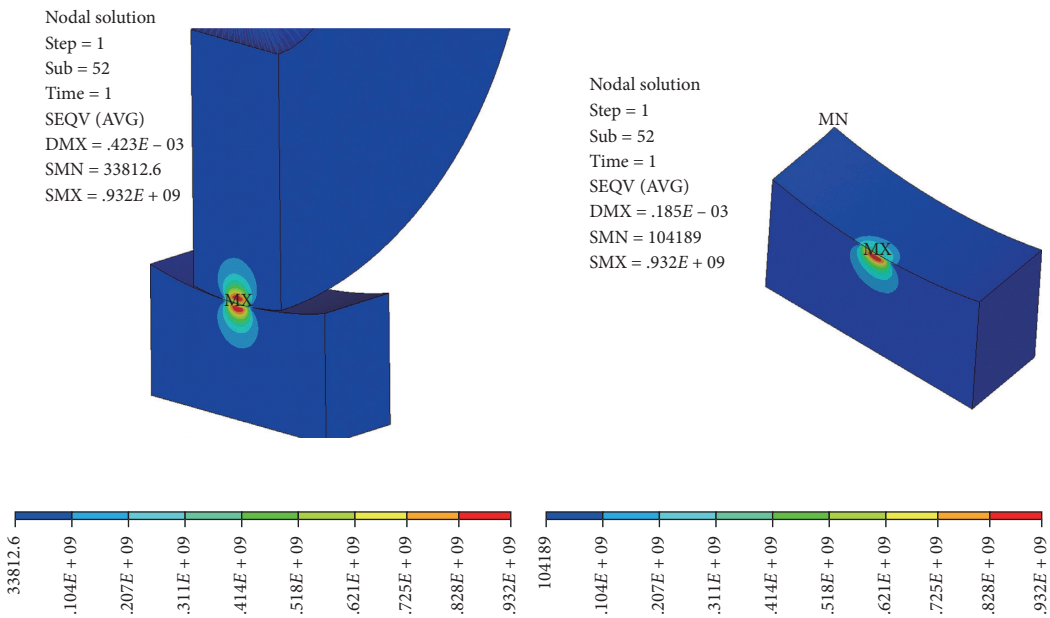

Figure 4: Equivalent stress distribution.

Table 2: Comparison of Hertz contact theory and finite-element simulation results.

Parameter	400 (kN)	800 (kN)	1200 (kN)	1600 (kN)	2000 (kN)
Hertz theoretical value (MPa)	1107	1395	1596	1757	1893
Contact stress simulation value (MPa)	1020	1300	1500	1670	1800
Equivalent stress simulation value (MPa)	634	807	932	1040	1110
Error between equivalent stress and theoretical value	7.85%	6.81%	6.01%	4.95%	4.91%
Distance between equivalent stress point and contact point (mm)	6.555	8.009	8.000	9.804	9.796

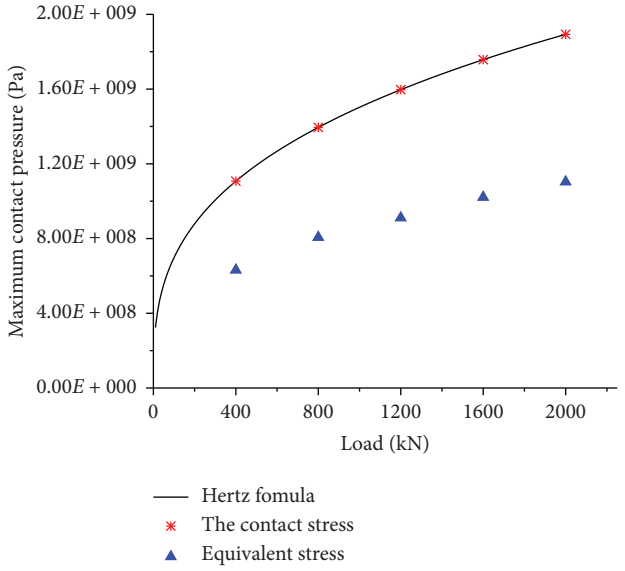

Figure 5: Relationship between maximum contact pressure and load.

weighted average of the known values of a spatial variable at several positions to estimate the value of the variable at other positions, to find an optimal linear unbiased estimate.

Table 3: Genetic algorithm parameters.

Parameter	Value
Group number	50
Crossover probability	0.8
Mutation rate	0.02
Repeat times	11300
Related functions	Gaussian function

Typically, computer-tested data consist of an input $\mathbf{X}$ and a response Y corresponding to the input. The response Y can be expressed as the sum of a linear model and the system deviation $Z(\mathbf{X})$:

$$Y(\mathbf{X}) = f(\mathbf{X}) + Z(\mathbf{X}), \tag{20}$$

where the remainder $Z(\mathbf{X})$ is considered independent and identically distributed, such as subject to a normal distribution. For the Kriging model, it can be expressed as

$$Y(\mathbf{X}) = \sum_{j=1}^{k} \beta_j f_j(\mathbf{X}) + Z(\mathbf{X}), \tag{21}$$

where $f_j(\mathbf{X})$ is the j_{th} known regression function. Normally, $f_j(\mathbf{X})$ can be taken as a fixed constant because its form does not determine the accuracy [28].

β_j is the correlation coefficient, expressed as a vector:

$$f(\mathbf{X}) = [f_1(\mathbf{X}), f_2(\mathbf{X}), \ldots, f_k(\mathbf{X})]^t, \quad (22)$$

$$\boldsymbol{\beta} = [\beta_1, \beta_2, \ldots, \beta_k]^t. \quad (23)$$

Also, Z(X) is considered a random process.

$$E(Z(\mathbf{X})) = 0, \mathrm{Cov}(Z(\mathbf{W}), Z(\mathbf{X})) = \sigma_z^2 \mathbf{R}(\mathbf{W}, \mathbf{X}). \quad (24)$$

In the expression, W and X represent any two sample points, σ_Z^2 is the process variance, and R(W, X)is a spatial correlation function. There are many choices forR(W, X). Generally, R(W, X)is taken in DACE (Design and Analysis of Computer Experiments) [29]:

$$\mathbf{R}(\mathbf{W}, \mathbf{X}) = \prod_{j=1}^{d} e^{-\theta |w_j - x_j|^p}, \quad (\theta \geq 0, 0 \leq p \leq 2). \quad (25)$$

In the abovementioned formula, j from 1 to d represents the dimension of the space, θ indicates how fast the correlation space function changes with |w-x|, and p indicates the smoothness of the model.

To simplify the symbols in the formula, we define

$$\mathbf{F} = \left[f^t(\mathbf{X}_1), f^t(\mathbf{X}_2), \ldots, f^t(\mathbf{X}_n)\right]^t, \quad (26)$$

$$\mathbf{R} = \left[\mathbf{R}\left(\mathbf{X}_i, \mathbf{X}_j\right)\right]_{m \times n}, \quad (27)$$

$$\mathbf{r}_\mathbf{x} = [\mathbf{R}(\mathbf{X}_1, \mathbf{X}), \mathbf{R}(\mathbf{X}_2, \mathbf{X}), \ldots, \mathbf{R}(\mathbf{X}_n, \mathbf{X})]^t. \quad (28)$$

Therefore, the best linear unbiased estimate for the unknown point B is

$$\hat{y}(x) = f_x^t \hat{\boldsymbol{\beta}} + \mathbf{r}^t(x)\mathbf{R}^{-1}(y - \mathbf{F}\hat{\boldsymbol{\beta}}), \quad (29)$$

where $\hat{\boldsymbol{\beta}} = (\mathbf{F}^t\mathbf{R}^{-1}\mathbf{F})^{-1}\mathbf{F}^t\mathbf{R}^{-1}y$ is the least-square estimate of $\boldsymbol{\beta}$.

The mean square deviation of $\hat{y}$ is

$$S(\hat{y}(\mathbf{X})) \approx \sigma_z^2\left(1 - \mathbf{r}_X^t\mathbf{R}^{-1}\mathbf{r}_X\right). \quad (30)$$

The parameter θ used to establish the Kriging model in equation (5) can be solved by the maximum unbiased estimation according to equation (7).

$$\max_{\theta>0} \phi(\theta) = \frac{\left[n \ln\left(\hat{\sigma}^2\right) + \ln|\mathbf{R}|\right]}{2}. \quad (31)$$

Thus, the construction problem of the optimal Kriging model is transformed into a nonlinear unconstrained optimization problem.

4.2. Genetic Algorithm Optimization. Genetic algorithm is a computational model that simulates the natural selection and genetic mechanism of Darwin's biological evolution theory. Its main feature is the use of a certain form of coding of decision variables as the object of operation. This way of encoding decision variables allows us to imitate the genetic and evolutionary incentives of organisms in nature and to conveniently apply genetic operators; the fitness function value transformed by the objective function value can be used to determine further the search range of the target function does not require other auxiliary information such as the derivative value of the objective function; the search process of the optimal solution starts from the initial population composed of many individuals, instead of starting from a single individual; it is an adaptive search technology, and its selection and operations such as crossover and mutation are all carried out in a probabilistic manner. Therefore, the genetic algorithm provides a general framework for solving complex system problems. It does not depend on the specific field of the problem and has strong robustness to the type of problem, so it is widely used in various fields [30–34]. The algorithm is simple, versatile, robust, and suitable for parallel processing.

As shown in Figure 6, the basic process of solving the global optimization problem using the genetic optimization algorithm based on the Kriging model [35–37] is as follows:

Step 1: the Latin hypercube selection method is used to select the parameters of the Kriging model and the initial sample points.

Step 2: a Kriging model is established and optimized with genetic algorithms to find the best point.

Step 3: the obtained points are checked, and it is determined if they meet the constraints and convergence conditions. If not, the point is deleted. If the point satisfies the constraint condition but does not satisfy the convergence condition, the first step is repeated. Then, the key points will be added to the initial sample site for the next optimized Kriging model. Also, if the point satisfies these two conditions, it becomes the best point.

4.3. Optimization of Structural Parameters of the Track Roller and Track Plate

4.3.1. Determining Design Variables. This paper aims to optimize the structural parameters of the roller and track plate under the condition that the width B of the roller and the track plate are constant. To meet the strength requirements, minimize the maximum contact stress in the contact area under heavy load conditions. The optimal design of the contact stress between the roller and the track plate is mainly determined by the following: the track roller radius R_1, the track roller rim radius r_1, and the track plate rim radius r_2. It is expressed in a matrix form as

$$X = \begin{bmatrix} x_1 \\ x_2 \\ x_3 \end{bmatrix} = \begin{bmatrix} r_1 \\ R_1 \\ r_2 \end{bmatrix}. \quad (32)$$

Range of values for each variable:

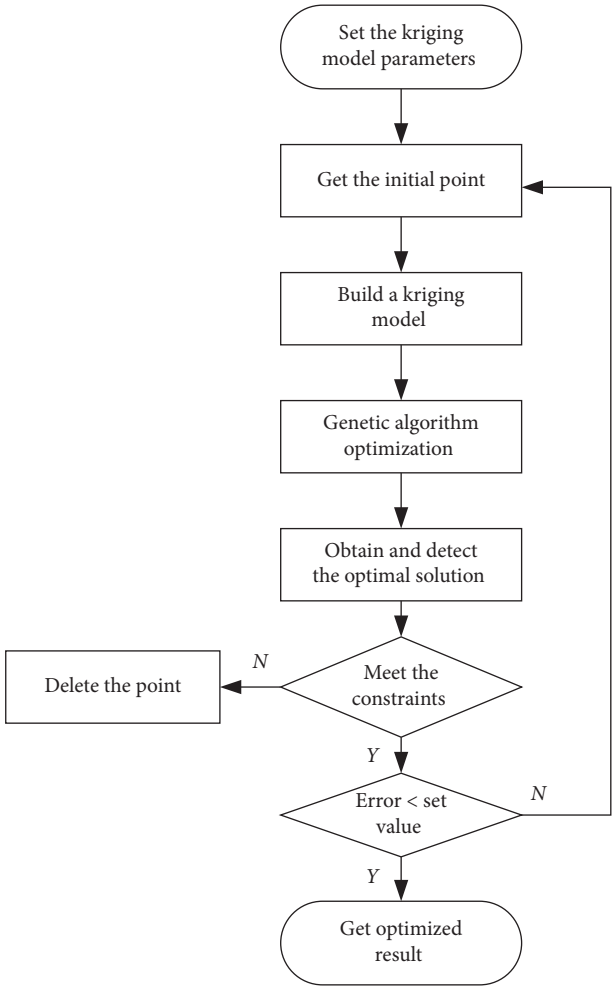

Figure 6: Optimization flow chart.

$$\begin{cases} 0.1 \le r_1 \le 2, \\ 0.12 \le r_2 \le 2.002, \\ 0.1 \le R_1 \le 0.8, \\ r_2 - r_1 \ge 0.002, \\ B = 0.2. \end{cases} \tag{33}$$

4.3.2. Establishing the Objective Function. When the roller and the track plate are in point contact, the abovementioned verification shows that the maximum stress of the contact area is approximately equal to the calculation result of the Hertz formula. Therefore, with the minimum contact stress as the optimization target, there is

$$f(X) = q_{\max H} = \frac{3}{2}\frac{P}{\pi ab}, \tag{34}$$

where P is the load on the roller, a is the elliptical long semiaxis of the contact area, and b is the elliptical short half of the contact area.

4.3.3. Determining Constraints. The most basic constraint is the contact strength constraint; that is, the maximum contact stress between the roller and the track plate is less than the allowable contact stress.

$$f(x) - p_{\text{Hper,sta}} \le 0. \tag{35}$$

4.3.4. Optimization Results. According to the abovementioned Kriging model, the parameters of the GA are set as Table 3.

When the load is set to 800 kN, the maximum contact stress for the optimal solution after 11300 iterations is $\min q_{\max} = 121.4$ MPa, and the stress value is much smaller than the allowable contact stress $p_{\text{Hper,sta}} = 2000$MPa. Also, this value is 91.30% lower than the maximum contact stress of 1395 MPa under the same size load in Table 2. The iterative process of each parameter of the roller and the track plate is shown in Figure 7.

The final structural parameters of the roller and track plate are shown in Table 4.

5. Discussion

5.1. Influence of Rim Radius Difference on Maximum Stress. When the roller and the track plate are in point contact, making the R_1 value at 0.6 m, the relationship between the load and the maximum contact stress P is shown in the curve of Figure 5. As the load increases, the maximum contact stress continues to rise. When the load is increased to a certain extent, the maximum contact stress increases slowly, but always increases.

The difference in the radius of the rim gradually decreases, and the relationship between the load and the maximum contact stress is shown in Figure 8. Under the same load, the maximum contact stress decreases sharply with the decrease of the radius difference of the rim. Therefore, in the design of the roller, the radius of the track roller rim and the radius of the cylindrical surface of the track plate can be selected to be nearly equal to reduce the maximum contact stress. At the same time, taking into account the environmental conditions, assembly efficiency, and plastic deformation in the working environment of the roller, it is recommended to maintain a 0.002–0.005 m radius difference during design and manufacture.

5.2. Relationship between Maximum Contact Stress and Rim Radius. When the radius of the roller rim is different from the radius of the cylindrical surface of the track plate by 0.02 m, the maximum contact stress with the radius under the load of 1000 kN is as shown in Figure 9. As the radius increases, the maximum contact pressure changes from a rapid decline to a slow decrease. Therefore, the radius r_1 and r_2 should be appropriately selected in the design; when the radius is too large, it will make the contact close to the plane contact, and too small radius will affect the maximum contact pressure.

5.3. Maximum Stress Comparison between Plane Contact and Arc Surface Contact. When the values of r_1 and r_2 tend to

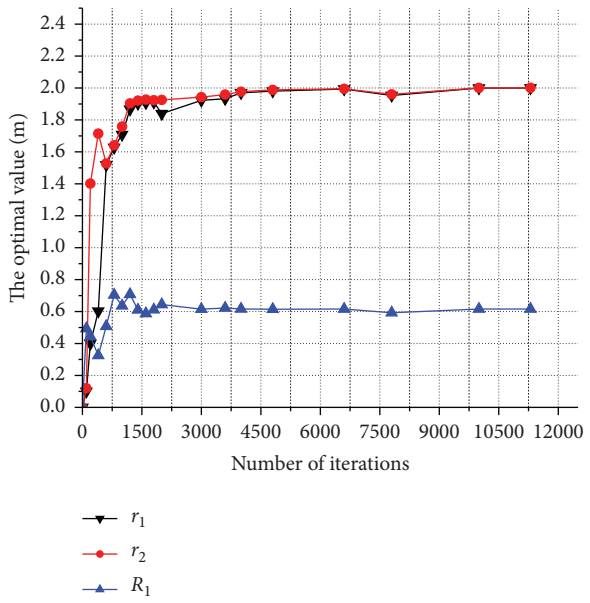

Figure 7: Generational variation of design variables.

Table 4: Optimized structural parameters.

Parameter	Value (m)
Track roller radius R_1	2.0011
Track roller rim radius r_1	2.0000
Track plate rim radius r_2	0.6158

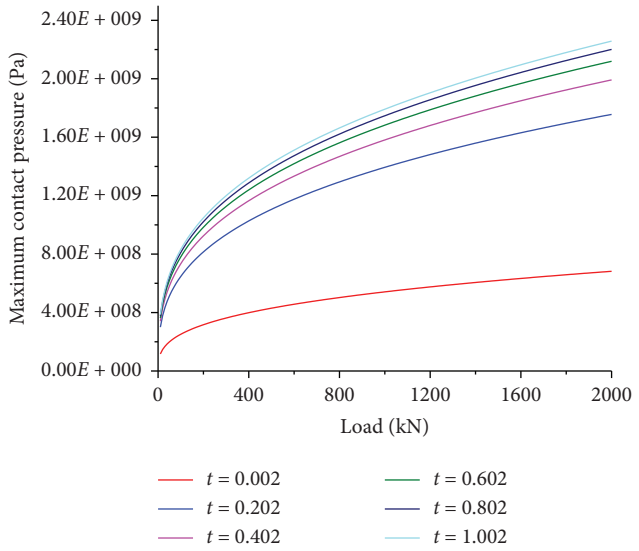

Figure 8: Influence of rim radius difference on maximum stress.

infinity, there is a plane line contact between the roller and the track plate. As shown in Figure 10, (a) is the line contact model of the roller and the track plate, and (b) is the enlarged view of the section of the line contact area; the contact area between these two changes from a point contact to a plane line contact, at which time the contact area is increased and the contact stress is reduced.

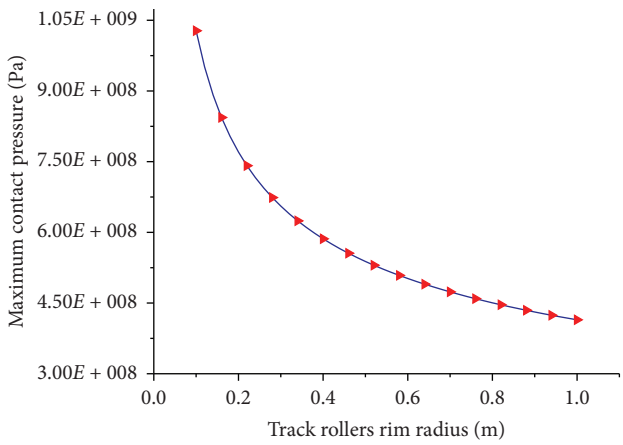

Figure 9: Relationship between maximum contact stress and rim radius.

The maximum contact stress of the line contact is taken as the objective function:

$$f(X) = q_{\max X} = 0.418 \times \sqrt{\frac{P \times E}{B \times R_1}}, \tag{36}$$

where B is the contact width of the roller and the track plate. In this paper, the contact width B is 0.2 m. E is the elastic modulus and has a value of 206 GPa.

When the rim radius r_1 of the roller and the radius r_2 of the track plate are close to each other, the contact area between the two increases, and the contact stress decreases. When the width of track roller is 0.2 m, r_1 is 1m, r_2 is 1.002 m, and $R_1 = 0.6$ m; the two curves in Figure 11 separately show the trend of the maximum contact stress in plane line contact and arc surface contact.

As shown in the abovementioned figure, when the load increases, the maximum contact stress of plane linear contact and arc surface contact increases. When the load is 180 kN, the maximum contact stress of the arc surface contact is equal to the maximum contact stress of the linear contact. When the load is less than 180 kN, the maximum contact stress of the plane line contact is slightly smaller than the arc surface contact. However, as the load increases continuously, after 180 kN, the maximum contact stress of the arc surface contact is significantly smaller than the maximum contact stress of the plane linear contact, and the difference between them is also increasing.

Table 5 lists the maximum contact stresses and their differences for the two structures when the loads are 400 kN, 800 kN, 1200 kN, 1600 kN, and 2000 kN, respectively. It can be seen from Table 5 that when the load is increased from 400 kN to 2000 kN, the maximum contact stress difference between the two structures is gradually increased from 12% to 33%.

It can be seen from the abovementioned results that when the load on the roller is large, the maximum contact stress of the arc surface contact is smaller than the maximum contact stress of the plane line contact. This is because the contact surface of the roller rim has a certain curvature, and when the difference between the rim radius r_1 of the roller and the

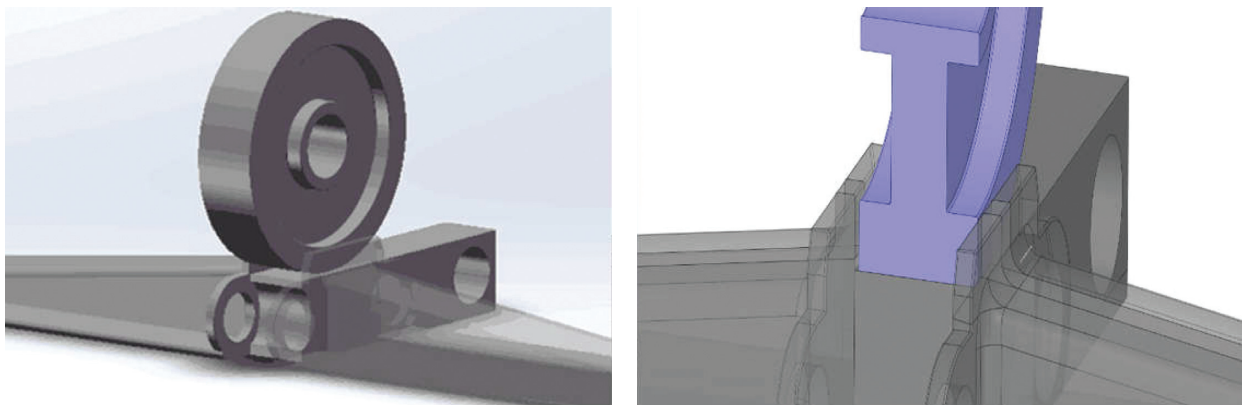

(a) (b)

Figure 10: The roller and the track plate are in plane line contact.

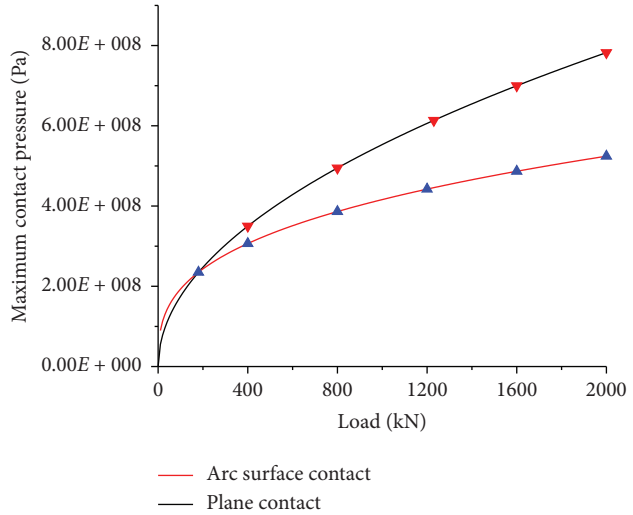

Figure 11: Comparison of maximum stress between plane contact and arc surface contact.

Table 5: Comparison of stress values between plane contact and arc surface contact.

Parameter	400 (kN)	800 (kN)	1200(kN)	1600 (kN)	2000 (kN)
Plane contact stress value (MPa)	350.0	494.8	606.0	699.8	785.4
Arc surface contact stress value (MPa)	305.3	384.7	440.4	484.7	522.1
Difference (%)	12.78	22.25	27.31	30.73	33.52

radius r_2 of the track plate is small, it is equivalent to transform the point contact into a line contact and increasing contact length between the roller and the track plate. Under the condition that the width of the roller is constant, the length of the arc line contact is longer than the length of the plane line contact. Therefore, in the design and manufacture of the roller, it is recommended to convert the planar contact into a curved contact. This can greatly reduce the maximum contact stress, ensure the work efficiency of the track walking mechanism, and improve the service life of the roller.

6. Conclusions

Based on Hertz contact theory, the mathematical model of point contact between the roller and track plate is established. Then, the Kriging model and the genetic algorithm are used to obtain the minimum surface contact pressure of the roller rim. On this basis, the relationship between the maximum contact stress and the structural parameters of the roller is discussed, and the structure shape of the roller is optimized.

(1) When the load is 800 kN, the genetic algorithm based on the Kriging model converges after 11300 iterations, and the optimal solution is obtained. At this time, the maximum contact stress is 121.40 MPa, which is 91.30% lower than the maximum contact stress of 1395 MPa under the same load in the second part of the verification model.

(2) The difference of the radius of the arc surface between the roller and the track plate affects the maximum contact stress of the roller. With the decrease of the radius difference of the arc surface, the maximum contact stress decreases gradually. When the radius difference is reduced to a certain extent, the maximum contact stress drops rapidly.

(3) When the contact surface between the roller and the track plate changes from a plane contact to a curved surface contact, the maximum contact stress can be reduced by up to 33.52%.

(4) When the rim radius of the roller and the track plate are similar, the maximum contact stress decreases sharply when the rim radius increases. After the rim radius continues to increase, the maximum contact stress changes to a slow drop.

Abbreviations

$R_{1,2}$: Radius of the track roller and track plate (m)
$r_{1,2}$,: Rim radius of the track roller and track plate (m)
$B_{1,2}$: Width of the track roller and track plate (m)
A_i, B_i: Parameters used in the derivation of the Hertzian stress formula
P: Load on the track roller (kN)
a: Ellipse long semiaxis of the contact area (m)
b: Ellipse short semiaxis of the contact area (m)
$K(k)$: First-class elliptic integral
$E(k)$: Second-class elliptic integral
Dk,C(k): Integrated elliptic integral
k: Elliptical eccentricity
$\nu_{1,2}$: Material Poisson's ratio of the track roller and track plate
$E_{1,2}$: Material elastic modulus of track roller and track plate (GPa)
δ: Displacement of the contact point between the track roller and the track plate (mm)
X: Input parameters of the Kriging model
Y: Input response of the Kriging model
$Z(X)$: System deviation in the Kriging model
$fj(X)$: The jth known regression function
βj: Correlation coefficient in the Kriging model
σz_2: Process variance in the Kriging model
$R(W,X)$: Spatial correlation coefficient, where W and X represent two random sample points
θ: An index which indicates how fast the value of the associated space function changes with w-x
p: Smoothness of the model
$y(x)$: Optimal linear unbiased estimation
β: Least-square estimation of β
Sy(X): Mean square deviation of y
$\max \phi(\theta)_{\theta>0}$: Maximum unbiased estimation of parameter θ of the Kriging model
qmaxH: Maximum contact stress calculated by the Hertz stress formula (Pa)
pHper,sta: Allowable contact static stress (MPa)
pHper,dyn: Allowable contact dynamic stress (MPa)
qmaxX: Maximum contact stress in line contact (MPa).

Data Availability

The data used to support the findings of this study are available from the corresponding author upon request.

Conflicts of Interest

The author declares that there are no conflicts of interest.

Acknowledgments

This work was funded by the Science and Technology Development Fund, Macau SAR (SKL-IOTSC-2018-2020).

References

[1] M. A. Arsić, S.-A. M Bošnjak, D. Zoran et al., "Analysis of the spreader track wheels premature damages," *Journal of Engineering Failure Analysis*, vol. 20, pp. 118–136, 2012.

[2] J. J. Zhao, H. Q. Tian, Y. Q. Ren, and Z. J. Lu, "Elastic and plastic analysis of drive wheel's Hertz contact," *Applied Mechanics and Materials*, vol. 184-185, pp. 188–195, 2012.

[3] T. W. Simpson, J. D. Poplinski, P. N. Koch, and J. K. Allen, "Metamodels for computer-based engineering design: survey and recommendations," *Engineering with Computers*, vol. 17, no. 2, pp. 129–150, 2001.

[4] T. W. Simpson, A. J. Booker, D. Ghosh, A. A. Giunta, P. N. Koch, and R. J. Yang, "Approximation methods in multidisciplinary analysis and optimization: a panel discussion," *Journal of Structural Multidisciplinary Optimizaiton*, vol. 27, no. 5, pp. 302–313, 2004.

[5] B. Wilson, D. Cappelleri, T. W. Simpson, and M. Frecker, "Efficient pareto frontier exploration using surrogate approximations," *Optimization and Engineering*, vol. 2, no. 1, pp. 31–50, 2001.

[6] G. Zhang, G. Wang, X. Li, and Y. Ren, "Global optimization of reliability design for large ball mill gear transmission based on the Kriging model and genetic algorithm," *Mechanism and Machine Theory*, vol. 69, pp. 321–336, 2013.

[7] M. A. Arslan, "3-D Rail-Wheel contact analysis using FEA," *Advances in Engineering Software*, vol. 45, no. 1, pp. 325–331, 2012.

[8] S. K. Sharma and A. Kumar, "Dynamics analysis of wheel rail contact using FEA," *Procedia Engineering*, vol. 144, pp. 1119–1128, 2016.

[9] G. Tao, Z. Wen, X. Zhao, and X. Jin, "Effects of wheel-rail contact modelling on wheel wear simulation," *Wear*, vol. 366-367, pp. 146–156, 2016.

[10] S. Javier, G. Vadillo Ernesto, and N. Correa, "On the influence of conformity on wheel–rail rolling contact mechanics," *Journal of Tribology International*, vol. 103, pp. 647–667, 2016.

[11] S.-H. Gao, G. Meng, and X.-H. Long, "Study of milling stability with Hertz contact stiffness of ball bearings," *Archive of Applied Mechanics*, vol. 81, no. 8, pp. 1141–1151, 2011.

[12] M. Olave, X. Sagartzazu, J. Damian et al., "Design of four contact-point slewing bearing with a new load distribution procedure to account for structural stiffness," *Journal of Mechanical Design*, vol. 132, no. 2, pp. 1–10, 2010.

[13] I. José, M. Pleguezuelos, and M. Muñoz, "Contact stress calculation of undercut spur and helical gear teeth," *Journal of Mechanism and Machine Theory*, vol. 46, no. 11, pp. 1633–1646, 2011.

[14] K. L/. Johnson, *Contact Mechanics*, Cambridge University Press, Cambridge, UK, 1987.

[15] S. Luo, Y. Wu, and J. Wang, "The generation principle and mathematical models of a novel cosine gear drive," *Mechanism and Machine Theory*, vol. 43, no. 12, pp. 1543–1556, 2008.

[16] S. Li, "Effect of addendum on contact strength, bending strength and basic performance parameters of a pair of spur gears," *Mechanism and Machine Theory*, vol. 43, no. 12, pp. 1557–1584, 2008.

[17] G. Vouaillat, J.-P. Noyel, F. Ville, X. Kleber, and S. Rathery, "From Hertzian contact to spur gears: analyses of stresses and rolling contact fatigue," *Mechanics & Industry*, vol. 20, no. 6, p. 626, 2019.

[18] D. Guyonneau, E. Mermoz, J. Mailhé, J.-M. Sprauel, and J.-M. Linares, "Stress optimization and study of the sensitivity to geometric variations of a spur gear tooth profile," *Mechanics & Industry*, vol. 14, no. 1, pp. 31–41, 2013.

[19] J. Liu, C. Tang, H. Wu, Z. Xu, and L. Wang, "An analytical calculation method of the load distribution and stiffness of an angular contact ball bearing," *Mechanism and Machine Theory*, vol. 142, Article ID 103597, 2019.

[20] J. Liu, Y. Xu, and G. Pan, "A combined acoustic and dynamic model of a defective ball bearing," *Journal of Sound and Vibration*, vol. 501, no. 1, p. 116029, 2021.

[21] N. Ichiro, *Elastic Mechanics Handbook*, Xi'an Jiaotong university publisher, Xi'an, China, 2014.

[22] Z. Yan, G. Wang, Z. Yao et al., "Contact analysis on huge crawler track wheel and track pad[J]," *Transactions of the Chinese Society of Agricultural Engineering*, vol. 28, no. 17, pp. 51–56, 2012.

[23] EN, *Steel Castings for General Engineering Uses*, European Committee for Standardization, Brussels, Belgium, 10293.

[24] *ANSYS Structural Analysis Guide*, ANSYS, Inc., Houston, TX, USA, 2004.

[25] N. Parida, S. K. Das, and S. Tarafder, "Failure analysis of railroad wheels," *Engineering Failure Analysis*, vol. 16, no. 5, pp. 1454–1460, 2009.

[26] J. Wang, H. Gao, and Y Zhou, *Kriging Address Drawing Technology - Computer Models and Algorithms*, Petroleum Industry Press, Beijing, China, 1998.

[27] S. Cagin, X. Fischer, É. Delacourt et al., "β-NTF reduction and fast kriging simulation of optimal engine configurations," *Mechanics & Industry*, vol. 18, no. 5, p. 509, 2017.

[28] W. J. Welch and T. J. Mitchell, "Wynn. Design and analysis of computer Experiments," *Statistics Science*, vol. 4, no. 4, pp. 409–435, 1989.

[29] I. Kaymaz, "Application of kriging method to structural reliability problems," *Structural Safety*, vol. 27, no. 2, pp. 133–151, 2005.

[30] J. Fernando and G. Wscher, "A MIP model and a biased random-key genetic algorithm based approach for a two-dimensional cutting problem with defects," *European Journal of Operational Research*, vol. 286, 2020.

[31] H. M. Pandey, "Secure medical data transmission using a fusion of bit mask oriented genetic algorithm, encryption and steganography," *Future Generation Computer Systems*, vol. 102, 2020.

[32] F. Guijarro, M. Martínez-Gómez, and D. Visbal-Cadavid, "A model for sector restructuring through genetic algorithm and inverse DEA," *Expert Systems with Applications*, vol. 154, no. 15, Article ID 113422, 2020.

[33] Z. Wang, F. Li, G. Shi et al., "network pruning using sparse learning and genetic algorithm," *Neurocomputing*, vol. 404, 2020.

[34] M. Salarkia, S. Golabi, and B. Amirsalari, "Optimum design of liquified natural gas Bi-lobe tanks using finite element, genetic algorithm and neural network," *Journal of Applied and Computational Mechanics*, vol. 6, no. 4, pp. 862–877, 2020.

[35] S. N. Lophaven, H. B. Nielsenc, and J. Sondergaard, "DACE: a matlab kriging toolbox," in *At Informatics and Mathematical Modelling*Technical University of Denmark, Lyngby, Denmark, 2002.

[36] J. Wang, M. Yao, and Y. Yang, "Global optimization of lateral performance for two-post-ROPS based on the kriging model and genetic algorithm," *Journal of Mechanical Engineering*, vol. 57, no. 10, pp. 760–767, 2011.

[37] S. Sakata, F. Ashida, and M. Zako, "Structural optimization using kriging approximation," *Computer Methods in Applied Mechanics and Engineering*, vol. 192, no. 7-8, pp. 923–939, 2003.